Marine Macrocyclic Imines, Pinnatoxins A and G: Structural Determinants and Functional Properties to Distinguish Neuronal α7 from Muscle α12$\beta\gamma\delta$ nAChRs.

Yves Bourne, Gerlind Sulzenbacher, Zoran Radić, Rómulo Aráoz, Morgane Reynaud, Evelyne Benoit, Armen Zakarian, Denis Servent, Jordi Molgó, Palmer Taylor, et al.

HHS Public Access

Author manuscript

Structure. Author manuscript; available in PMC 2016 June 02.

Published in final edited form as:

Structure. 2015 June 2; 23(6): 1106–1115. doi:10.1016/j.str.2015.04.009.

Marine macrocyclic imines, pinnatoxins A and G: structural determinants and functional properties to distinguish neuronal α7 from muscle $\alpha 1_2\beta\gamma\delta$ nAChRs

Yves Bourne[1,2,*,†], **Gerlind Sulzenbacher**[1,2,†], **Zoran Radiæ**[3], **Rómulo Aráoz**[4,5], **Morgane Reynaud**[5], **Evelyne Benoit**[4,5], **Armen Zakarian**[6], **Denis Servent**[5], **Jordi Molgó**[4,5], **Palmer Taylor**[3], and **Pascale Marchot**[1,2,*]

[1]Aix-Marseille Université, Laboratoire Architecture et Fonction des Macromolécules Biologiques, Campus Luminy, 13288 Marseille cedex 9, France

[2]Centre National de la Recherche Scientifique, Laboratoire Architecture et Fonction des Macromolécules Biologiques, Campus Luminy, 13288 Marseille cedex 9, France

[3]Department of Pharmacology, Skaggs School of Pharmacy and Pharmaceutical Sciences, University of California San Diego, La Jolla, CA 92093-0650, USA

[4]Neuro-PSI, Institut des Neurosciences Paris-Saclay, Centre National de la Recherche Scientifique, Bât. 32-33, 91190 Gifsur-Yvette, France

[5]Commissariat à l'Energie Atomique, iBiTecS, Service d'Ingénierie Moléculaire des Protéines, Laboratoire de Toxinologie Moléculaire et Biotechnologies, 91191 Gif-sur-Yvette, France

[6]Department of Chemistry and Biochemistry, University of California Santa Barbara, CA 93106-9510, USA

Abstract

Pinnatoxins are macrocyclic imine phycotoxins associated with algal blooms and shellfish toxicity. Functional analysis of pinnatoxin-A and pinnatoxin-G, by binding and electrophysiology on membrane-embedded neuronal α7, α4β2 and α3β2 and muscle-type $\alpha 1_2\beta\gamma\delta$ nicotinic acetylcholine receptors (nAChRs), reveals high-affinity binding and potent antagonism for the α7

*Corresponding authors: yves.bourne@afmb.univ-mrs.fr; pascale.marchot@univ-amu.fr.
†**Authors YB and GS** contributed equally to the structural part of this study.

Author contributions. YB, DS, JM, PT, PM designed the research; YB, GS, ZR, RA, MR, PM performed the experiments; YB, GS, ZR, EB, DS, JM, PT, PM analyzed the data; YB, ZR, DS, JM, PT, PM wrote the paper.

Accession codes. The atomic coordinates and structure factors of the pinnatoxin-A and pinnatoxin-G complexes with *Aplysia californica* AChBP have been deposited with the RCSB Protein Data Bank (www.rcsb.org) and attributed PDB accession codes, 4XHE and 4XK9, respectively.

Supplemental Information

Supplemental Information includes Supplemental Introduction, Supplemental Data, Supplemental Experimental Procedures, Supplemental References, two Supplemental figures and two Supplemental tables and can be found with this article online at http://.....

and $\alpha 1_2\beta\gamma\delta$ subtypes. The toxins also bind to the nAChR surrogate, acetylcholine-binding protein (AChBP), with low K_d's reflecting slow dissociation. Crystal structures of pinnatoxin-AChBP complexes (1.9–2.2Å resolution) picture the multiple anchoring points of the hydrophobic portion, the cyclic imine and the substituted *bis*-spiroketal and cyclohexene ring systems of the pinnatoxins that dictate tight binding between the opposing loops C and F at the receptor subunit interface, as observed for the 13-desmethyl-spirolide-C and gymnodimine-A congeners. Uniquely however, the bulky bridged EF-ketal ring specific to the pinnatoxins extends radially from the interfacial-binding pocket to interact with the sequence-variable loop F and govern nAChR-subtype selectivity and central neurotoxicity.

Graphical Abstract

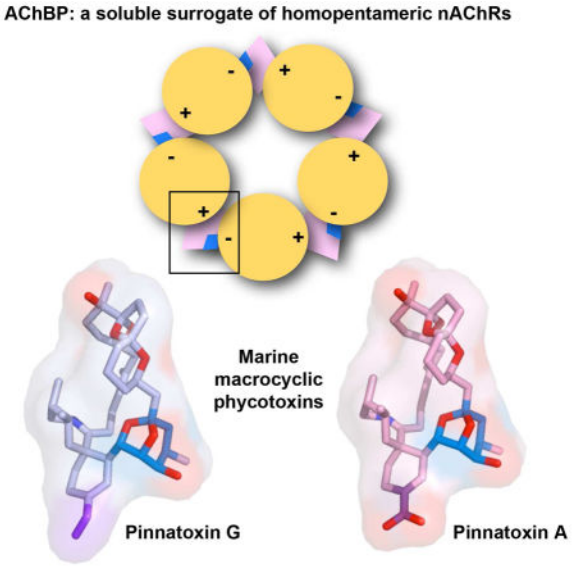

Keywords

acetylcholine binding protein; competitive antagonism; crystal structure; macrocyclic imine; dinoflagellate toxin; marine phycotoxin; nicotinic acetylcholine receptor; pinnatoxin; nAChR subtype; seafood poisoning; subunit interface

Introduction

The "rapid-acting" macrocyclic imines toxins consist of a recently identified and widely distributed group of phycotoxins with increasing prevalence in warming oceanic environments (Stivala et al., 2015). Among them, pinnatoxins (Fig. 1) and pteriatoxins represent one of the largest subgroups of 27-membered macrocyclic imine phycotoxins first detected in coastal Japan and isolated from the digestive glands of the bivalve mollusks *Pinna attenuata* and *Pinna muritica* (pinnatoxins A-D) (Zheng et al., 1990; Uemura et al., 1995) and *Pteria penguin* (pteriatoxins A-C) (Takada et al., 2001). Novel congeners (pinnatoxins E-G) were rapidly isolated from a range of shellfish samples from Australia and New Zealand, and pinnatoxin-G (PnTx-G) was proposed to represent a biosynthetic

progenitor for all pinnatoxins, as exemplified by metabolic oxidation of PnTx-G into pinnatoxin-A (PnTx-A) after ingestion by shellfish (Selwood et al., 2010). PnTx-A and PnTx-G, along with iso-spirolide C and 20-methyl spirolide G, are widespread in shellfish samples from Norwegian waters (Rundberget et al., 2011). Pinnatoxins and pteriatoxins contain the 7-membered spirocyclic imine structure common to most spirolides, but an unusual 6,5,6-*bis*-spiroketal moiety replaces the spirolide 5,5,6 ring system (reviewed in (Molgó et al., 2014; Otero et al., 2011; Stivala et al., 2015)). They also contain a bulky bridged 5,6-bicycloketal substructure instead of a smaller allylic alcohol linker and a quaternary stereocenter at the core of the spiroimine ring, along with varying functional group substitutions. Fatty acid ester metabolites of PnTx-G were recently identified in mussels from Eastern Canada and these esterified forms may display higher toxicity (McCarron et al., 2012).

Numerous shellfish-poisoning instances have been attributed to these bioactive alkaloids, and PnTx-A has been proposed as one of the major compounds responsible for a poisoning outbreak in China and Japan (Zheng et al., 1990). When administered intraperitoneally or orally to mice, all (+)-pinnatoxin congeners so far identified induce rapid lethality associated with central neurological symptoms (Selwood et al., 2010) and flaccid paralysis (Aráoz et al., 2011) suggesting action at Ca^{2+}-channels and/or acetylcholine receptors. They also display the highest oral toxicity among cyclic imine toxins (Munday et al., 2012). In fact, the high oral toxicity of pinnatoxin F compared to the E and G congeners (Fig. 1) has raised recent concerns about possible adverse effects for shellfish consumers (Munday et al., 2012). In contrast, the non-natural (−)-PnTx-A is inactive in mouse assays (Munday R, 2008). Identification of successful strategies for the synthesis of (+)-PnTx-A and PnTx-G, and subsequent electrophysiological, competition binding and computational analyses established PnTx-A as a potent antagonist of nicotinic acetylcholine receptors (nAChR), with high selectivity for the human neuronal α7 subtype (Stivala and Zakarian, 2008; Nakamura et al., 2008; Aráoz et al., 2011). In contrast, a synthetic aminoketone derivative of PnTx-A (PnTx-A AK) with an open imine ring shows no action on various nAChR subtypes, a feature supporting the central role of the imine ring for potent nAChR antagonism previously observed for the related toxins, 13-desmethyl spirolide C (SPX) and gymnodimine A (GYM) (Aráoz et al., 2011; Bourne et al., 2010). Hence, the unusual stability of the imine ring in pinnatoxins has implications for their potent toxicity when administered orally (Jackson et al., 2012).

The nAChRs are prototypical cation-selective, ligand-gated ion channels that mediate fast neurotransmission in the central and peripheral nervous systems (Changeux, 2012). They belong to the Cys-loop superfamily of the ligand-gated ion channels and are formed by distinct combinations of five subunits that confer selectivity in pharmacological properties and regional tissue locations. The diversity in the nAChR subunit subtypes and assemblies is most evident in the central nervous system where up to nine α and three β subunits have been described (Le Novère et al., 2002). The various receptors used in this study are briefly described in the Supplementary Information (SI) and their subunit sequences are displayed in Suppl. Fig. S1.

The soluble acetylcholine (ACh) binding proteins (AChBP) from mollusks form homopentameric assemblies of subunits homologous to the N-terminal, extracellular ligand-binding domain of the nAChR (Brejc et al., 2001; Hansen et al., 2002; Celie et al., 2004) (Suppl. Fig. S1). In addition to the overall structural features of the subunits, the aromatic side chains that form the ligand binding pocket at the subunit interfaces are well conserved in the nAChR family, with greater variation of residues at the complementary (or (−)) face than at the principal (or (+)) face of each interface. The binding pocket of AChBP possesses all the functional residues identified in the nAChR ligand-binding domain, and its extension towards apical and "membrane" directions along the interface provides multiple means for selective accommodation of nicotinic full and partial agonists and competitive antagonists (Celie et al., 2004; Hansen et al., 2005; Hibbs et al., 2009). Overall, agonists recognize a "core agonist signature motif" central to the binding pocket, whereas the larger antagonists extend towards the apical or the membrane directions, resulting in opening of loop C on the (+) face, and often in greater subtype selectivity than seen for agonists. Novel α7/AChBP chimeras harboring a fully functional α7-like ligand-binding site show a marked enhancement in ligand affinity correlated with conservation of the overall architecture, thus justifying their use for investigating ligands selective for the neuronal α7 subtype (Li et al., 2011; Nemecz and Taylor, 2011).

Previously we documented the mode of binding of two closely related macrocyclic imine toxins, SPX and GYM, to *Aplysia californica* and *Lymnaea stagnalis* AChBPs (A- and L-AChBP) and showed why they are extremely potent nicotinic antagonists with broad specificity toward various nAChR subtypes (Bourne et al., 2010). In particular, crystal structures of the SPX- and GYM-A-AChBP complexes revealed neatly imbedded phycotoxins within the AChBP nest of aromatic side chains that accommodates all nicotinic agonists and competitive antagonists. Predominant interactions were observed with residues in loop C from the (+) face of the subunit interface but only sparing interactions with residues in loop F on the (−) face, consistent with loop F dictating nAChR subtype specificity. Moreover, the protonated imine nitrogen in the toxins exhibits tight hydrogen bonding with the backbone carbonyl oxygen of loop C residue Trp147 on the (+) face in AChBP. The requirements for hydrogen bonding orientation and distance (~3.0 Å) constrain the orientation of the toxin core centered within the pocket. More recent investigations involving several nAChR subtypes and muscarinic receptors along with complementary binding and molecular docking studies confirmed the nAChRs as the primary targets of SPX and GYM with no significant binding to a wide range of other receptors (Hauser et al., 2012).

To delineate experimentally the molecular determinants that govern the unique selectivity of PnTx-A for the neuronal α7 nAChR and to explore the capacity of PnTx-G for subtype selectivity, we conducted a comprehensive pharmacological and structural study of chemically synthesized PnTx-A, PnTx-G and the PnTx-A AK derivative, relative to the neuronal α7, α4β2 and α3β2 and muscle-type $\alpha 1_2\beta\gamma\delta$ nAChRs and to A- and L-AChBP and the previously developed α7/AChBP chimera III with enhanced α7 binding properties (Nemecz and Taylor, 2011). Our data, when compared with those reported for the SPX and GYM toxins, point to the bicyclic EF-ketal ring found in the pinnatoxins (Fig. 1) as a novel

binding determinant for mediating polar *versus* non-polar interactions with loop F that confers nAChR subtype selectivity, and extend toxicological insights for these prevalent marine biotoxins.

Results and Discussion

Functional and binding characteristics and nAChR subtype selectivity of PnTx-A and PnTx-G

Functional analyses of PnTx-A and PnTx-G were performed by voltage-clamp recording of ACh-evoked currents in oocytes expressing the neuronal α7 or α4β2 nAChRs or in oocytes microtransplanted with the muscle-type nAChR. PnTx-A blocked the current in both neuronal nAChRs without affecting the desensitization rates, although with a ~300-fold greater potency (denoted by the IC_{50} values) and apparent irreversibility toward α7 (Aráoz et al., 2011) (Fig. 2, Suppl. Fig. S2A, Table 1). PnTx-G also blocked these currents but, compared with PnTx-A, it displayed ~50-fold lower potency towards α7 and no selectivity between the two neuronal subtypes. Both PnTx-A and PnTx-G also blocked the ACh-evoked current in the membrane-bound muscle-type $\alpha 1_2\beta\gamma\delta$ nAChR, with nanomolar potencies equivalent to that of PnTx-G for the two neuronal nAChRs. Hence, the inhibitory potency of PnTx-A depends on the nAChR subtype, with IC_{50} values in the 0.1–10 nM range and a $\alpha 7 > \alpha 1_2\beta\gamma\delta > \alpha 4\beta 2$ ranking in selectivity, while those values of PnTx-G lie in the same nanomolar range for all three nAChR subtypes. Finally, analysis of the open-ring PnTx-A AK derivative led to IC_{50} values in the sub-millimolar range for the three nAChR subtypes, consistent with the initial report of their absence of activity (Aráoz et al., 2011).

Binding analyses were performed in the membrane-bound muscle-type $\alpha 1_2\beta\gamma\delta$ nAChR and in mammalian cells transiently expressing the neuronal α7 (as a α7/5-HT3 chimera), α4β2 and α3β2 nAChRs, by competition against radiolabeled derivatives of the competitive antagonist α-bungarotoxin (BgTx) and the full agonist (+/−)-epibatidine (EPI), respectively (Aráoz et al., 2011) (Suppl. Fig. S2B, Table 2). Similar sub-nanomolar binding potencies (denoted by the K_i values) of PnTx-A and PnTx-G were obtained for the α7 nAChR, whereas potencies ranging from 10 to100 nM where recorded for the α4β2 and α3β2 subtypes, pointing to selectivity of PnTx-A and PnTx-G for the homopentameric α7 *versus* heteropentameric neuronal nAChRs. By contrast, on the muscle-type nAChR, PnTx-G interacted with 25-fold higher affinity than PnTx-A, leading to a rank ordering of $\alpha 7 > \alpha 1_2\beta\gamma\delta > \alpha 3\beta 2 \sim \alpha 4\beta 2$ and $\alpha 1_2\beta\gamma\delta > \alpha 7 > \alpha 3\beta 2 \sim \alpha 4\beta 2$ in the PnTx-A and PnTx-G specificities, respectively. Analysis of the PnTx-A AK derivative led to K_i values greater than 1–10 μM, consistent with the electrophysiological analyses.

Finally, complementary binding analyses were performed using mammalian cells stably expressing the neuronal α7 or α4β2 nAChRs along with a Ca^{2+} sensing fluorescent tag (Yamauchi et al., 2011) (Table 3). PnTxA binding to the α7 nAChR led to a K_d value similar to the IC_{50} and K_i values obtained upon voltage-clamp and competitive binding experiments (Table 1 and Table 2, respectively), whereas PnTx-A binding to the α4β2 nAChR and PnTx-G binding to either receptor led to more divergent values, presumably because of the distinct methodological approaches and time required to reach equilibrium

conditions. Yet, for both toxins the same α7 > α4 ranking in selectivity reported above was retained.

Hence, the higher blocking potencies and higher binding affinities of PnTx-A and PnTx-G for the neuronal α7 and muscle-type $\alpha 1_2\beta\gamma\delta$ nAChRs, respectively, compared with the two neuronal heteropentameric nAChRs, should arise from distinguishing structural determinants in pinnatoxins.

Binding characteristics of PnTx-A and PnTx-G with A- and L-AChBPs and a α7/A-AChBP chimera

The sequence differences and distinctive binding affinities of the two AChBPs for the nicotinic ligands render them useful templates for studying ligand binding to various nAChR subtypes (Table 4). Binding of nicotinic agonists and competitive antagonists to A- and L-AChBPs, in affecting the connectivity of the aromatic side chains in the binding pocket, is associated with quenching of the intrinsic Trp fluorescence (Hansen et al., 2002). Quenching is sufficient to monitor rates of complex formation and dissociation by stopped-flow kinetic instrumentation and to correlate the ratio of dissociation and association rates with the dissociation constants measured by equilibrium titrations with ligand. To ascertain kinetic constants for slow dissociating complexes and confirm the equilibrium constants for the lower affinity complexes, a complementary scintillation proximity assay was also used.

Binding data for PnTx-A and PnTx-G reveal K_d values in the 10^{-7} M range for L-AChBP but in the 10^{-11}–10^{-9} M range for A-AChBP, with differences being primarily governed by the dissociation rates (k_{off}). The association rates approach the diffusion limitation for partly sequestered sites and show smaller differences between AChBP species (Table 4). In fact, PnTx-A binding to A-AChBP, with its dissociation constant below 50 pM and its >3400-fold selectivity over L-AChBP, approaches the characteristics of SPX binding kinetics for A-AChBP (Bourne et al., 2010), while PnTx-G binding appears only slightly less favorable (420-fold in selectivity). In contrast, binding of the PnTx-A AK derivative to A- and L-AChBP led to K_d values in the mM range, confirming the critical role of the cyclic imine to confer high potency binding. However, PnTx-G binding to the α7/A-AChBP chimera mutant III, expected to reflect binding properties intermediate to the α7 nAChR and A-AChBP (Nemecz and Taylor, 2011), involved 10-fold lower affinity, indicating that sequential mutagenesis cannot yield a full complement of residues to achieve the folding differences between the two proteins.

Hence, both PnTx-A and PnTx-G show higher affinity binding for A-AChBP over L-AChBP, with PnTx-A accounting for the greater selectivity and reflecting a similar preference for neuronal α7 nAChR. These features justify the use of A-AChBP for structural analyses.

Overall view of the crystalline PnTx-AChBP complexes

The crystal structures of PnTx-A and PnTx-G bound to A-AChBP, solved at 1.9 Å and 2.2 Å resolution, respectively, show the compact homopentameric ring assembly of subunits found in all AChBP structures (Fig. 3, Suppl. Table S1) (reviewed in (Karlin, 2002; Sixma and Smit, 2003)). The ligand binding pocket encompasses a nest of five electron-rich

aromatic side chains provided by residues Tyr93 in loop A, Trp147 in loop B and Tyr188 and Tyr195 in loop C on the (+) face of the interface, and residue Tyr55 in loop D on the (−) face (Suppl. Fig. S1). The pocket is partially sheltered from the solvent by loop C, which is found at the outer perimeter of the pentamer and harbors at its tip the vicinal disulfide bridge linking the vicinal Cys190 and Cys191 residues, a signature determinant for nAChR α subunits. The well-defined electron densities reveal fully occupied subunit interfaces with identical orientations of all five PnTx-A or PnTx-G bound within a pentamer (Fig. 3), consistent with their sub-nanomolar affinities and low dissociation rates for A-AChBP (Table 1) (cf rmsd values in the Experimental Procedures). Each toxin molecule, shaped as a slightly curved crescent of overall dimensions 14 × 6 × 6 Å, tightly accommodates the curvature of the subunit interface, resulting in buried surface areas of ~380 $Å^2$ and ~370 $Å^2$ at the (+) and (−) faces of the interface, respectively (Fig. 3, Table 3).

Detailed description of the PnTx-AChBP complexes

PnTx-A, with its sub-nanomolar IC_{50}, K_i and K_d values for the α7 nAChR and A-AChBP (Tables 1–3), shows higher specificity for these receptors over PnTx-G, which in turn appears to be more selective for the muscle-type nAChR. Despite the close resemblance of the two A-AChBP complexes, structural differences contributed by the distinctive R^1 substituent (carboxylate in PnTx-A *versus* vinyl in PnTx-G, Fig. 1) in the two toxins may well account for the functional differences.

At the subunit interfaces in both complexes, the bulky spirolide skeleton is oriented with its long axis aligned roughly parallel to the five-fold axis of the pentamer (Fig. 3). The 6,5,6 *bis*-spiroketal three-ring system (rings BCD on Fig. 1), being bulkier than the 6,5,5 *bis*-spiroketal found in SPX, points in an apical direction along the interface while the R^1-substitued cyclohexene ring (ring G), located at the opposite end of the molecule, is oriented in the membrane direction of the subunit interface. The *bis*-spiroketal framework bends toward the central protonated cyclic imine ring (ring A) and comfortably complements the shape of the binding pocket. This orientation of the carbon skeleton ideally positions the cyclic imine centrally to the subunit interface and within hydrogen bonding distance (~2.9 Å for PnTx-A and 2.8 Å for PnTx-G) to the carbonyl oxygen of Trp147 in A-AChBP loop B (Suppl. Fig. S1, Table S2), as found for the corresponding imines in SPX and GYM (~2.9 Å). The two vicinal methyl groups on the cyclic imine, also found in SPX, largely contribute to binding by abutting against the conserved phenol rings of Tyr188 and Tyr195 from loop C. Ideal positioning of the central cyclic imine in the binding pocket is consistent with absence of binding of the open-ring PnTx-A AK derivative to A- and L-AChBPs and the nAChR subtypes assayed (Tables 1–3).

On the apical side of the interface, the *bis*-spiroketal system emerges from the macrocyclic framework and abuts against the tip of loop C, where it buttresses the binding interface (Fig. 3). Here, this ring system perfectly complements the non-polar environment of the surrounding residues in A-AChBP, and retains the preferred *cis* stereochemistry elucidated by NMR analysis and confirmed by total synthesis (Chou, 1996; McCauley et al., 1998). As a result, the proximal tetrahydropyran ring (ring D) perfectly abuts against Tyr188, Tyr195 and the vicinal Cys190 and Cys191 (loop C), while the central tetrahydrofuran ring (ring C)

does not make direct contacts, and while the distal tetrahydropyran ring (ring B) interacts with Val148 (loop E) from the (−) face. Here, the hydroxyl and methyl substituents on the distal tetrahydropyran ring are respectively positioned to make a hydrogen bond with Tyr195 (loop C) and van der Waals contacts with Arg79 and Val108 (loop E). The additional methyl and hydroxyl groups that distinguish ring D of PnTx-D from the other congeners could alter the degree of closure of loop C.

In the membrane direction of the interface, the cyclohexene ring (ring G) in PnTx-A and PnTx-G makes nearly edge-to-face stacking interactions with Tyr93 (loop A) from the (+) face and Tyr55 (loop D) from the (−) face (Fig. 3). The carboxylate group (R^1 substituent) in PnTx-A, much smaller than the corresponding (γ)-butyrolactone moiety in SPX and GYM, is perfectly positioned to hydrogen bond with Ser167 (loop F) and make several water-mediated contacts with Tyr188 (loop C). By contrast, the corresponding vinyl group in PnTx-G establishes weak interactions only with Ser167, since its more non-polar character does not permit formation of the solvation shell associated with bound PnTx-A. The mode of interaction of the PnTx R^1 substituent in AChBP is consistent with a reduced *in vitro* neuromuscular blocking activity and *in vivo* toxicity of a fluorophore-conjugated PnTxF derivative at this position (Hellyer et al., 2014).

In the solvent-exposed surface, the bulky bridged 5,6-bicycloketal substructure (ring EF), which is unique to the pinnatoxins and pteriatoxins, radially extends from the binding pocket to promote additional interactions with the complementary face (Fig. 3). Hence, the exocyclic hydroxyl (R^2 substituent) and methyl groups of the pinnatoxins mediate interactions with Thr36 in strand β1, Ile118 in loop E and Asp164 in loop F, along with water-mediated interactions between the hydroxyl group and the cluster of polar residues Asp164, Ser166 and Ser167 in loop F.

Comparison of the modes of binding of the pinnatoxins, spirolides and gymnodimines

Structural features of the A-AChBP complex with PnTx-A and PnTx-G closely resemble those observed for the SPX and GYM complexes (cf. rmsd values in *Experimental Procedures*). Indeed, deep anchoring of PnTx-A and PnTx-G at the subunit interface results in a buried surface increase of ~750 $Å^2$ (1.4 Å probe radius), close to the ~680 $Å^2$ and ~600 $Å^2$ surface areas buried by bound SPX and GYM, respectively (Bourne et al., 2010) (Fig. 4). Also, comparative analysis of the buried surface at the binding pockets shows a significant contribution of the bridged 5,6-bicycloketal (ring EF) in PnTx-A and PnTx-G, which is replaced by a smaller allylic alcohol linker in SPX and GYM, along with subtle variations around the R^1 group at the base of the cyclohexene ring. The additional exocyclic hydroxyl (R^3) and methyl (R^4) groups in the tetrahydropyran ring (ring D) of the pinnatoxins D, E and F may lead to steric clashes with the facing Tyr188 and Tyr195 phenyl rings and require conformational adaptability of loop C associated with distinct binding properties. Concomitant variability in the R^1 group and absence of the hydroxyl group (R^2) in the bridged bicycloketal substructure that faces the complementary subunit surface may significantly affect the potency and subtype selectivity of the three pinnatoxin congeners. Most importantly, the bicycloketal substructure (ring EF), located in the solvent-exposed branch of PnTx-A and PnTx-G and harboring exocyclic hydroxyl (R^2) and methyl groups,

distinguishes the pinnatoxins and pteriatoxins (cf. below) from the spirolides and gymnodimines. Compared to the methyl and hydroxyl groups found in SPX at positions 9 and 10, respectively, this substructure offers additional interactions and water-mediated contacts with Asp164 and the neighboring Ser166-Ser167 residue pair in the sequence-variable loop F (Figs. 3 and 4). The acyl chain at position C28 in the bridged 5,6-bicycloketal (EF) substructure of the esterified pinnatoxin conjugates may generate steric clashes with residues in loop F, with significant reductions in binding affinities for the AChBPs and nAChRs.

Other members of this emerging biotoxin family, such as the structurally related pteriatoxins, would be expected to bind in a similar way as PnTx-A and PnTx-G. Compared with the pinnatoxins, the pteriatoxins contain the same 6,5,6-*bis*-spiroketal and 5,6-bicycloketal rings, but they differ in the chemical properties of the R^1 group that extends from the cyclohexene G ring at the bottom of the macrocyclic framework. This moiety, that replaces the (γ)-butyrolactone ring in SPX and GYM, extends toward the membrane side of the binding pocket where a highly ordered network of solvent molecules connects neighboring residues at the (−) face. In methyllycaconitine (MLA), the bulkier N-phenyl succinimide moiety, which represents a major determinant for α7 selectivity, overlaps only partially with the R^1 group of PnTx (Fig. 4) (García-Guzmán et al., 1995).

Structure-activity implications for PnTx binding to L-AChBP and the nAChRs

The presence of a Trp residue in loop D of L-AChBP and most nAChRs, in place of Tyr55 in A-AChBP, most likely contributes to the >3400- and ~400-fold lower affinities of PnTx-A and PnTx-G, as documented for other ligands (Hansen et al., 2004; Hansen et al., 2005; Hibbs et al., 2009; Bourne et al., 2010; Rucktooa et al., 2012; Edink et al., 2011). As well, the side chains of Tyr164 in loop F and neighboring Lys36 in strand β1, being bulkier than the corresponding Ser167 and Thr36 side chains in A-AChBP (Fig. 4, Suppl. Fig. S1), are likely to encounter steric clashes with the exocyclic methyl and hydroxyl groups in the 5,6-bicycloketal ring (ring EF) of PnTx-A and PnTx-G and contribute to the lower affinity for L-AChBP (Table 3).

Proximity of the sequence-variable loop F region, at the (−) face of the binding pocket, to the cyclohexene ring harboring the R^1 group with differences in charge (e.g. carboxylate *versus* vinyl), along with additional substructures in the various pinnatoxin congeners, clearly are key functional determinants in the pinnatoxins for dictating selectivity toward the α7 or $\alpha 1_2\beta\gamma\delta$ nAChRs compared to the α3β2 and α4β2 nAChRs (Tables 1 and 2). Hence, replacement of A-AChBP loop F residue Ser167 (Gly167 in human and chicken α7, Ala in δ subunit of the *Torpedo* nAChR) to a charged Asp residue in the β2 subunits may contribute to the low affinity of PnTx-A and PnTx-G for the neuronal heteropentameric nAChRs. The recent crystal structure of the LBD of the neuronal α9 subunit bound to MLA in a monomeric state pointed to the lack of interaction of the N-phenyl succinimide moiety at the bottom of the binding pocket with shorter side chains Thr147 and I190 (corresponding to bulkier AChBP Q186 and K143) (Zouridakis et al., 2014). Molecular diversity amongst the PnTx congeners, as exemplified by a lactone ring attached to the cyclohexene ring in PnTx-F instead of a carboxylate in PnTx-A or vinyl group in PnTx-G, may contribute to the

highest potency of PnTx-F in acute toxicity studies (Munday et al., 2012). Yet, lack of a hydroxyl group in the bridged EF-ketal ring of PnTx-D, PnTx-E and PnTx-F could modulate interactions with residues from the complementary subunit at the base of the binding pocket and contribute to nAChR selectivity.

Hence, these structures confirm the importance of the cyclic imine and *bis*-spirocetal framework embedded within a macrocyclic skeleton as key determinants to confer high binding affinity and potent nAChR antagonism to the pinnatoxins, as previously documented for the spirolides and gymnodimines (Bourne et al., 2010). In contrast to the limited interactions of the latter two toxins with the sequence-variable loop F to preserve broad nAChR subtype specificity, the structures also point to the key role of the radially protruding bicycloketal ring (ring EF) unique to the pinnatoxins to promote an additional, either polar or non-polar, interaction network with loop F and govern subtype selectivity.

Concluding remarks

The pinnatoxins are members of the expanding superfamily of macrocyclic imine biotoxins that are structurally related to the previously characterized non-selective SPX and GYM toxins. Yet they contain unique substituents that target distinct structural determinants located on the (−) face of the subunit interface of the nAChRs and their AChBP surrogates and confer subtype selectivity. Indeed, all these phycotoxins embed a cyclic 6 or 7-membered imine ring structure that tethers the toxin core at a pivotal place and displays exquisite shape and chemical complementarity with the ligand-binding pocket, while the unique substructures of the macrocyclic framework of the pinnatoxins radially extend from the binding pocket to engage in distinctive interactions with residues from the complementary face and the sequence-variable loop F of the nAChRs. This study unveils the specific positions of the functional variations in the substituents attached to the macrocyclic framework and offers new concepts for the design of new ligands with higher nAChR subtype selectivity. Since most other subtype-selective nAChR antagonists, such as the conotoxins, are polar molecules that do not cross the blood–brain barrier, the macrocyclic imine framework also offers new avenues for distinguishing nAChR subtype functions in the brain.

Experimental Procedures

Live animals and biological materials

Their sources are stated in the Supplementary Information.

Concentration-inhibition analysis of ACh currents

The procedures for nAChR microtransplantation and expression in oocytes and for voltage-clamp recording are described in the SI. Dose-response curves for agonist activation were analyzed using equation: $I = I_{max}[L]^n/(EC_{50} + [L])^{nH}$ (equ. 2), where I is the measured agonist-evoked current, [L] is the agonist concentration, EC_{50} is the agonist concentration that evoked half the maximal current (I_{max}) and nH is the Hill coefficient. Current (I) values were normalized to the I_{max} value recorded from the same oocyte to yield fractional (%) response data. IC_{50} values were determined from dose-response curves by fitting to

equation: $F = 1/[1+([X]/IC_{50})^{nH}]$ (equ. 3), where F is the fractional response obtained in presence of the inhibitor at concentration [X] and IC_{50} is the inhibitor concentration that reduced the ACh-evoked amplitude by half. Statistical significance of differences between controls and test values was assessed using the two-tailed Student's t-test or the Kolmogorov-Smirnov two-sample test and $p < 0.05$. Data are presented in Fig. 2, Suppl. Fig. S2A, and Table 1.

Binding assays on the nAChRs

The procedures for preparation of *T. marmorata* membranes enriched in the muscle-type $\alpha 1_2\beta\gamma\delta$ nAChR and for transient expression of the human neuronal $\alpha 3\beta 2$ and $\alpha 4\beta 2$ nAChRs and chicken $\alpha 7$/mouse 5-HT3 chimera from tsA-201 cells are described in the SI. Equilibrium competition on $\alpha 1_2\beta\gamma\delta$ used 0.05 μg of membranes (~100 pM in toxin binding sites), 0.5–1.5 nM ^{125}I-bungarotoxin (BgTx) (L*) and a range of PnTx concentrations (at least 4 h incubation, 20–25°C) (Servent et al., 1997). Equilibrium competition on the $\alpha 7$/5-HT3 chimera and $\alpha 3\beta 2$ and $\alpha 4\beta 2$ nAChRs used a cell density adjusted to specifically bind no more than 10% of the radioligand ^{125}I-BgTx ($\alpha 7$/5-HT3) or [^{3}H]-epibatidine (EPI) ($\alpha 3\beta 2$ and $\alpha 4\beta 2$), added at 0.9–0.5 nM (~25–30-fold the K_d, see below) (L*), and a range of PnTx concentrations (4 h incubation, 20–25°C) (Kharrat et al., 2008). IC_{50} values were determined by fitting the competition data to a binding isotherm and conversion to K_i constants using equation: $K_i = IC_{50}/(1+L^*/K_d)$ (equ. 1) (Cheng and Prusoff, 1973), and K_d values of 50 pM for ^{125}I-BgTx binding on $\alpha 1_2\beta\gamma\delta$ and of 35 pM and 20 pM for [^{3}H]-EPI binding on $\alpha 3\beta 2$ and $\alpha 4\beta 2$, respectively. Data are presented in Suppl. Fig. S2B and Table 2.

Stable Ca^{2+} sensing nAChR cell lines and binding assays

Stable Ca^{2+} sensing tsA-201 cell lines (CNiFER) (Yamauchi et al., 2011) expressing human 7 or 42 nAChRs were harvested at 70–80% of confluence with a light trypsin treatment. They were diluted with Hank's Balanced Salt Solution (HBSS) buffer containing 1% BSA to a cell count of ~5–10,000 per ml and plated in 0.02ml into a 96-well low-profile plate. [^{3}H]-EPI, wheat germ agglutinin, scintillation proximity assay beads (Amersham Biosciences) (~100 μg/well) and specified concentrations of competing toxin in HBSS buffer in 1% BSA were added to each well to a final volume of 80 μl. Plates were incubated at room temperature for 2 h before repetitive counting on a Wallac 1450 Microbeta Trilux counter. Data were analyzed by GraphPad Prism 4 and fitted to a sigmoidal concentration-response curve to determine IC_{50} and K_d values. They are presented in Table 3.

Ligand binding to AChBPs and the α7/A-AChBP chimera

The procedures for stable expression and purification of AChBPs and the $\alpha 7$/A-AChBP chimera are described in the SI. Rate constants for association (k_{on}) and dissociation (k_{off}) were determined by multiple kinetic means to cover the wide range of values observed, as previously described (Hansen et al., 2002; Hansen et al., 2005). Measurement of k_{on}'s (and k_{off}'s in case of lower affinity ligands) entailed direct admixture of reactants and monitoring the quenching of the protein native Trp fluorescence. Additional measurements of k_{off} employed occupation of free AChBP binding sites by a competing ligand (gallamine) in excess over its K_d, to form a non-quenching complex. In brief, each equilibrated PnTx-

AChBP complex at 250 pM in binding sites and slight molar excess of toxin was mixed with [^{3}H]-MLA for A-AChBP or [^{3}H]-EPI for L-AChBP at concentrations well above their respective K_d value to titrate those binding sites made available upon toxin dissociation. The time course of [^{3}H]-ligand binding was monitored over several hours. First order dissociation rate constants were determined by nonlinear regression of data using simple mono-exponential relationship. $K_{d/calc}$ values were derived from the ratio of rate constants. Data are presented in Table 4.

Structure determination and refinement

The procedures for complex formation and crystallization and for data collection are described in the SI. The structures were solved by molecular replacement with PHASER (McCoy et al., 2006) using the apo A-AChBP structure (PDB code 2BYN (Hansen et al., 2005)) as a search model. Analysis of the binding site in a preliminary difference map of the PnTx-A AK complex revealed five empty interfaces in an otherwise well-ordered AChE pentamer, consistent with the extremely low binding affinity of the derivative (Table 4). The initial PnTx-AChBP models were improved by manual adjustment with COOT (Emsley and Cowtan, 2004) and were refined with REFMAC (Murshudov et al., 1997) including TLS refinement with each subunit defining a TLS group. In each case, a random set of reflections was set aside for cross-validation purposes. The molecular structures of PnTx-A and PnTx-G and the associated library files containing stereochemical and parametric data were generated with SKETCHER (CCP4, 1994). Automated solvent building used COOT. Data collection and refinement statistics are reported in Suppl. Table S1.

The final structures comprise A-AChBP residues His1-Arg208 for each of the five subunits in the two pentamers in the asymmetric unit and a fully resolved PnTx-A or PnTx-G molecule in each of the ten binding sites. The N-terminal FLAG sequence (cf. above) is fully resolved in one subunit of each pentamer, while high temperature factors and weak electron density are associated with the other FLAG sequences and with surface loop Asn15-Met19 in all subunits. The stereochemistry of the structures was analyzed with COOT and MOLPROBITY (Davis et al., 2007).

Structural analyses and comparisons

Comparison of the PnTx-A and PnTx-G AChBP complexes with other structures include those of A-AChBP in the apo form and as complexes with the phycotoxins SPX and GYM (PDB codes 2WZY and 2X00 (Bourne et al., 2010)) and the diterpene alkaloid from plant, MLA (PDB code 2BYR (Hansen et al., 2005)). The average root mean square deviation between AChBP subunits bound to PnTx-A and PnTx-G is 0.3 Å for 208 Cα atoms; between AChBP bound to PnTx-A and the above-mentioned structures it is in the 0.36–0.67 Å range for 212–216 Cα atoms.

Supplementary Material

Refer to Web version on PubMed Central for supplementary material.

Acknowledgments

We gratefully acknowledge the expert assistance of: Kwok-Yiu Ho, Kimberly Gomez and Dr. John Yamauchi (UCSD, La Jolla) for AChBP, α7 and α4β2 binding assays; Sandrine Conrod (CNRS/AMU, Marseille) for crystallization; the ID14-4 staff of the European Synchrotron Radiation Facility (ESRF, Grenoble) and the Proxima-1 staff of the SOLEIL synchrotron (Gif-sur-Yvette) during data collection. This work was supported by grant NIH/NIGMS R01 GM077379 (to AZ); grant AQUANEUROTOX-ANR-12-ASTR-0037 (to JM and DS); USPHS grants R37-GM18360 and P42-ES-010337 (to PT); the French Infrastructure for Integrated Structural Biology (FRISBI) ANR-10-INSB-05-01 (to the AFMB lab); and a CNRS-DRI PICS grant (to YB and PM).

References

Aráoz R, Servent D, Molgó J, Iorga BI, Benoit E, Gu Z, Stivala C, Zakarian A. Total synthesis of pinnatoxins A and G and a revision of the mode of action of pinnatoxin A. J Am Chem Soc. 2011; 133:10499–10511. [PubMed: 21644584]

Bourne Y, Radiæ Z, Aráoz R, Talley TT, Benoit E, Servent D, Taylor P, Molgó J, Marchot P. Structural determinants in phycotoxins and AChBP conferring high affinity binding and nicotinic AChR antagonism. Proc Natl Acad Sci U S A. 2010; 107:6076–6081. [PubMed: 20224036]

Brejc K, van Dijk WJ, Klaassen RV, Schuurmans M, van Der Oost J, Smit AB, Sixma TK. Crystal structure of an ACh-binding protein reveals the ligand-binding domain of nicotinic receptors. Nature. 2001; 411:269–276. [PubMed: 11357122]

CCP4. The CCP4 suite: Programs for protein crystallography. Acta Crystallogr D Biol Crystallogr. 1994; 50:760–763. [PubMed: 15299374]

Celie PH, van Rossum-Fikkert SE, van Dijk WJ, Brejc K, Smit AB, Sixma TK. Nicotine and carbamylcholine binding to nicotinic acetylcholine receptors as studied in AChBP crystal structures. Neuron. 2004; 41:907–914. [PubMed: 15046723]

Changeux JP. The nicotinic acetylcholine receptor: the founding father of the pentameric ligand-gated ion channel superfamily. J Biol Chem. 2012; 287:40207–40215. [PubMed: 23038257]

Cheng Y, Prusoff WH. Relationship between the inhibition constant (K1) and the concentration of inhibitor which causes 50 per cent inhibition (I50) of an enzymatic reaction. Biochem Pharmacol. 1973; 22:3099–3108. [PubMed: 4202581]

Chou T. Relative stereochemistry of pinnatoxin A, a potent shellfish poison from *Pinna muricata*. Tetrahedron Letters. 1996; 37:4023–4026.

Davis IW, Leaver-Fay A, Chen VB, Block JN, Kapral GJ, Wang X, Murray LW, Arendall WB, Snoeyink J, et al. MolProbity: all-atom contacts and structure validation for proteins and nucleic acids. Nucleic Acids Res. 2007; 35:W375–W383. [PubMed: 17452350]

Edink E, Rucktooa P, Retra K, Akdemir A, Nahar T, Zuiderveld O, van Elk R, Janssen E, van Nierop P, et al. Fragment growing induces conformational changes in acetylcholine-binding protein: a structural and thermodynamic analysis. J Am Chem Soc. 2011; 133:5363–5371. [PubMed: 21322593]

Emsley P, Cowtan K. Coot: model-building tools for molecular graphics. Acta Crystallogr D Biol Crystallogr. 2004; 60:2126–2132. [PubMed: 15572765]

García-Guzmán M, Sala F, Sala S, Campos-Caro A, Stühmer W, Gutiérrez LM, Criado M. α-Bungarotoxin-sensitive nicotinic receptors on bovine chromaffin cells: molecular cloning, functional expression and alternative splicing of the α7 subunit. Eur J Neurosci. 1995; 7:647–655. [PubMed: 7620615]

Hansen SB, Radiæ Z, Talley TT, Molles BE, Deerinck T, Tsigelny I, Taylor P. Tryptophan fluorescence reveals conformational changes in the acetylcholine binding protein. J Biol Chem. 2002; 277:41299–41302. [PubMed: 12235129]

Hansen SB, Sulzenbacher G, Huxford T, Marchot P, Taylor P, Bourne Y. Structures of *Aplysia* AChBP complexes with nicotinic agonists and antagonists reveal distinctive binding interfaces and conformations. EMBO J. 2005; 24:3635–3646. [PubMed: 16193063]

Hansen SB, Talley TT, Radiæ Z, Taylor P. Structural and ligand recognition characteristics of an acetylcholine-binding protein from *Aplysia californica*. J Biol Chem. 2004; 279:24197–24202. [PubMed: 15069068]

Hauser TA, Hepler CD, Kombo DC, Grinevich VP, Kiser MN, Hooker DN, Zhang J, Mountfort D, Selwood A, et al. Comparison of acetylcholine receptor interactions of the marine toxins, 13-desmethylspirolide C and gymnodimine. Neuropharmacology. 2012; 62:2239–2250. [PubMed: 22306792]

Hellyer SD, Selwood AI, van Ginkel R, Munday R, Sheard P, Miles CO, Rhodes L, Kerr DS. In vitro labelling of muscle type nicotinic receptors using a fluorophore-conjugated pinnatoxin F derivative. Toxicon. 2014; 87:17–25. [PubMed: 24887283]

Hibbs RE, Sulzenbacher G, Shi J, Talley TT, Conrod S, Kem WR, Taylor P, Marchot P, Bourne Y. Structural determinants for interaction of partial agonists with acetylcholine binding protein and neuronal α7 nicotinic acetylcholine receptor. EMBO J. 2009; 28:3040–3051. [PubMed: 19696737]

Jackson JJ, Stivala CE, Iorga BI, Molgó J, Zakarian A. Stability of cyclic imine toxins: interconversion of pinnatoxin amino ketone and pinnatoxin A in aqueous media. J Org Chem. 2012; 77:10435–10440. [PubMed: 23116445]

Karlin A. Emerging structure of the nicotinic acetylcholine receptors. Nat Rev Neurosci. 2002; 3:102–114. [PubMed: 11836518]

Kharrat R, Servent D, Girard E, Ouanounou G, Amar M, Marrouchi R, Benoit E, Molgó J. The marine phycotoxin gymnodimine targets muscular and neuronal nicotinic acetylcholine receptor subtypes with high affinity. J Neurochem. 2008; 107:952–963. [PubMed: 18990115]

Le Novère N, Corringer PJ, Changeux JP. The diversity of subunit composition in nAChRs: evolutionary origins, physiologic and pharmacologic consequences. J Neurobiol. 2002; 53:447–456. [PubMed: 12436412]

Li SX, Huang S, Bren N, Noridomi K, Dellisanti CD, Sine SM, Chen L. Ligand-binding domain of an α7-nicotinic receptor chimera and its complex with agonist. Nat Neurosci. 2011; 14:1253–1259. [PubMed: 21909087]

McCarron P, Rourke WA, Hardstaff W, Pooley B, Quilliam MA. Identification of pinnatoxins and discovery of their fatty acid ester metabolites in mussels (*Mytilus edulis*) from Eastern Canada. J Agric Food Chem. 2012; 60:1437–1446. [PubMed: 22239716]

McCauley JA, Nagasawa K, Lander PA, Mischke SG, Semones MA, Kishi Y. Total synthesis of pinnatoxin A. J Am Chem Soc. 1998; 120:7647–7648.

McCoy JG, Arabshahi A, Bitto E, Bingman CA, Ruzicka FJ, Frey PA, Phillips GN. Structure and mechanism of an ADP-glucose phosphorylase from *Arabidopsis thaliana*. Biochemistry. 2006; 45:3154–3162. [PubMed: 16519510]

Molgó, J.; Aráoz, RI.; Benoit, E.; Iorga, BI. Seafood and freshwater toxins. Pharmacology physiology and detection. CRC Press; 2014. Cyclic imine toxins: chemistry, origin, metabolism, pharmacology, toxicology, and detection; p. 951-990.

Munday R, Selwood AI, Rhodes L. Acute toxicity of pinnatoxins E, F and G to mice. Toxicon. 2012; 60:995–999. [PubMed: 22813782]

Munday, R. Seafood and Freshwater Toxins: Pharmacology, Physiology and Detection. CRC Press; 2008. Toxicology of cyclic imines: gymnodimine, spirolides, pinnatoxins, pteriatoxins, prorocentrolide, spiro-prorpcentrimine, and symbiomines; p. 581-594.

Murshudov GN, Vagin AA, Dodson EJ. Refinement of Macromolecular Structures by the Maximum-Likelihood Method. Acta Crystallogr D Biol Crystallogr. 1997; 53:240–255. [PubMed: 15299926]

Nakamura S, Kikuchi F, Hashimoto S. Total synthesis of pinnatoxin A. Angew Chem Int Ed Engl. 2008; 47:7091–7094. [PubMed: 18666279]

Nemecz A, Taylor P. Creating an α7 nicotinic acetylcholine recognition domain from the acetylcholinebinding protein: crystallographic and ligand selectivity analyses. J Biol Chem. 2011; 286:42555–42565. [PubMed: 22009746]

Otero A, Chapela MJ, Atanassova M, Vieites JM, Cabado AG. Cyclic imines: chemistry and mechanism of action: a review. Chem Res Toxicol. 2011; 24:1817–1829. [PubMed: 21739960]

Rucktooa P, Haseler CA, van Elk R, Smit AB, Gallagher T, Sixma TK. Structural characterization of the binding mode of smoking cessation drugs to nicotinic acetylcholine receptors through the study of ligand complexes with acetylcholine binding protein. J Biol Chem. 2012; 287:23283–23293. [PubMed: 22553201]

Rundberget T, Aasen JA, Selwood AI, Miles CO. Pinnatoxins and spirolides in Norwegian blue mussels and seawater. Toxicon. 2011; 58:700–711. [PubMed: 21920377]

Selwood AI, Miles CO, Wilkins AL, van Ginkel R, Munday R, Rise F, McNabb P. Isolation, structural determination and acute toxicity of pinnatoxins E, F and G. J Agric Food Chem. 2010; 58:6532–6542. [PubMed: 20408554]

Servent D, Winckler-Dietrich V, Hu HY, Kessler P, Drevet P, Bertrand D, Ménez A. Only snake curaremimetic toxins with a fifth disulfide bond have high affinity for the neuronal α7 nicotinic receptor. J Biol Chem. 1997; 272:24279–24286. [PubMed: 9305882]

Sixma TK, Smit AB. Acetylcholine binding protein (AChBP): a secreted glial protein that provides a high-resolution model for the extracellular domain of pentameric ligand-gated ion channels. Annu Rev Biophys Biomol Struct. 2003; 32:311–334. [PubMed: 12695308]

Stivala CE, Zakarian A. Total synthesis of (+)-pinnatoxin A. J Am Chem Soc. 2008; 130:3774–3776. [PubMed: 18311987]

Stivala CE, Benoit E, Aráoz R, Servent D, Novikov A, Molgó J, Zakarian A. Synthesis and biology of cyclic imine toxins, an emerging class of potent, globally distributed marine toxins. Nat Prod Rep. 2015; 32:411–435. [PubMed: 25338021]

Takada N, Umemura N, Suenaga K, Uemura D. Structural determination of pteriatoxins A, B and C, extremely potent toxins from the bivalve Pteria penguin. Tetrahedron Letters. 2001; 42:3495–3497.

Uemura D, Chou T, Haino T, Nagatsu A, Fukuzawa S, Zheng S, Chen H. Pinnatoxin A: a toxic amphoteric macrocycle from the Okinawan bivalve *Pinna muricata*. J Am Chem Soc. 1995; 117:1155–1156.

Yamauchi JG, Nemecz Á, Nguyen QT, Muller A, Schroeder LF, Talley TT, Lindstrom J, Kleinfeld D, Taylor P. Characterizing ligand-gated ion channel receptors with genetically encoded Ca^{2++} sensors. PLoS ONE. 2011; 6:e16519. [PubMed: 21305050]

Zheng SZ, Huang FL, Chem SC, Tan XF, Zuo JB, Peng J, Xie RW. The isolation and bioactivities of pinnatoxin. Chin J Mar Drugs. 1990; 9:33–55.

Zouridakis M, Giastas P, Zarkadas E, Chroni-Tzartou D, Bregestovski P, Tzartos SJ. Crystal structures of free and antagonist-bound states of human α9 nicotinic receptor extracellular domain. Nat Struct Mol Biol. 2014; 21:976–980. [PubMed: 25282151]

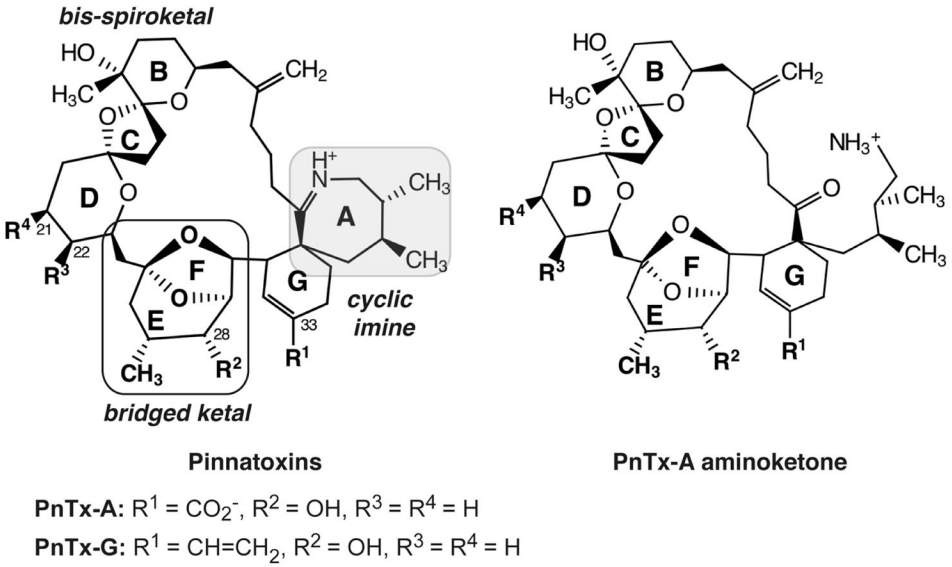

Fig. 1. Chemical structures of the pinnatoxin variants and the open-ring PnTx-A AK derivative

The 7-membered cyclic imines common to other spirolides are highlighted with a grey background while the substructures that distinguish the pinnatoxins from other spirolides are boxed. Locations of group substitutions (R^1 to R^4) that differ amongst the various pinnatoxins are indicated. PnTx-A: $R^1 = CO_2$, R^2 = OH, $R^3 = R^4$ = H; PnTx-G: R^1 = $CH=CH_2$/O-acyl esters (C14 to C24 acyl chain with variable numbers of double bonds), R^2 = OH, $R^3 = R^4$ = H; PnTx-B/C: $R^1 = NH_2CO_2$, R^2 = OH, $R^3 = R^4$ = H; PnTx-D: R^1 = $CO(CH_2)_2CO_2$, R^2 = H, R^3 = OH, $R^4 = CH_3$; PnTx-E: $R^1 = COH(CH_2)_2CO_2$, R^2 = H, R^3 = OH, $R^4 = CH_3$; PnTx-F: $R^1 = C_4H_6O_2$ (butyrolactone), R^2 = H, R^3 = OH, $R^4 = CH_3$.

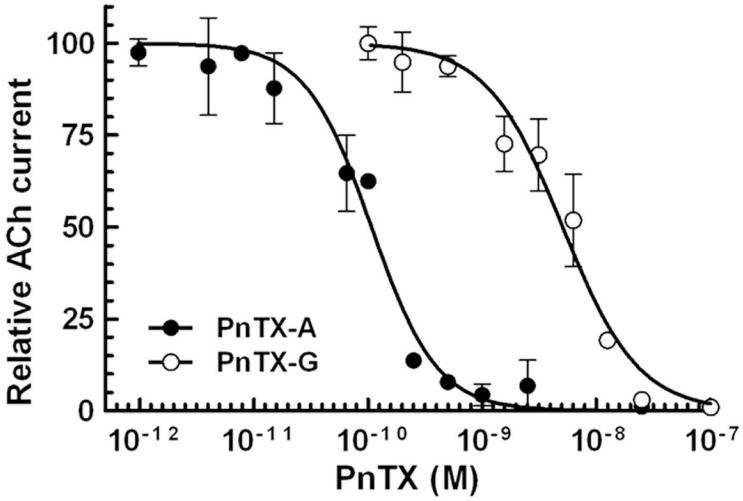

Fig. 2. Inhibition of ACh-evoked currents recorded from human α7 nAChR transiently expressed in oocytes

The amplitudes of the ACh-induced currents recorded in the presence of PnTx-A (filled circles) and of PnTx-G (empty circles) (mean ± SEM; 3–4 oocytes per concentration) were normalized to control currents and are expressed as relative current values. The holding membrane potential during recordings was −60 mV.

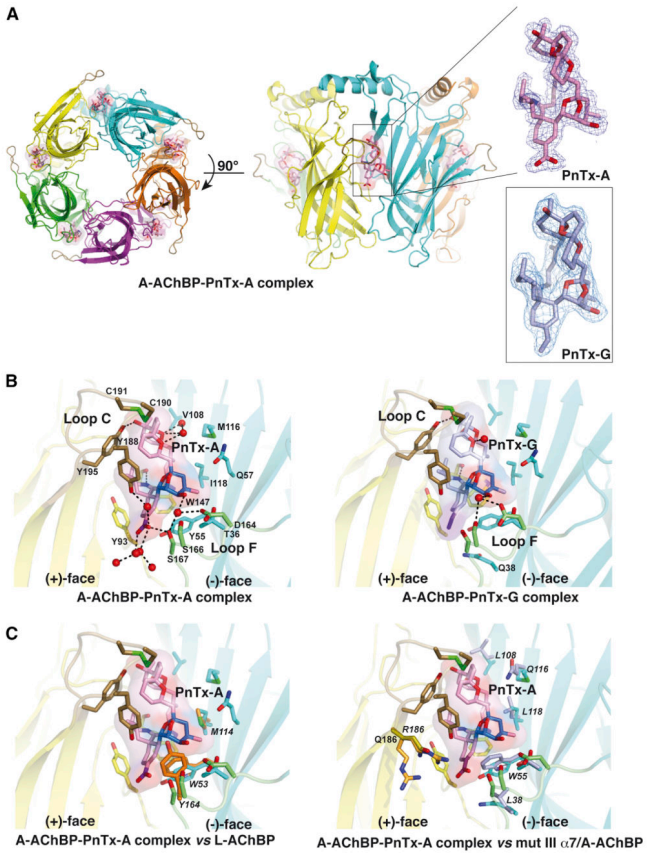

Fig. 3. Overall and close-up views of the pentameric PnTx-AChBP complexes, and structural comparisons

(A) The pentamer in the PnTx-A complex is viewed from the "membrane" side (left), and in a radial perspective towards one subunit interface with the apical side at top and the membrane side at bottom (center). The main and side chains at the (+) and (−) faces of the exemplified interface are displayed in yellow and cyan, respectively. The position and orientation of bound PnTx-A and PnTx-G are identical. Bound PnTx-A (pink bonds and molecular surface, red oxygens, blue nitrogen) and PnTx-G (light blue bonds and molecular surface, red oxygens, blue nitrogen) are perfectly ordered, as assessed by the quality of the 1.9Å and 2.2 Å resolution 2Fo-Fc electron density maps contoured at 1.2σ (blue) (right).

(B) Close-up views of bound PnTx-A (left) and PnTx-G (right) in the aromatic nest at the subunit interface, showing details of the cyclic imine environment (radial perspective). The Cys190-Cys191 disulfide bridge embedded at the tip of loop C is displayed in brown and loop F is in green. The 5,6-bicycloketal ring (i.e., ring EF in Fig. 1) is highlighted in blue. Side chains (in yellow and cyan) and solvent molecules (red dots) that interact specifically with bound PnTx-A/G are shown and labeled. The dashed lines denote hydrogen bonds. Note the distinctive interaction networks of the R^1 substituents at the membrane side of the interface.

(C) Overlays of A-AChBP as bound to PnTx-A with L-AChBP (PDB code 1UW6) (left) and the α7/A-AChBP chimera mutant III (PDB code 3SH1) (right). Residues in the ligand-binding pockets of L-AChBP and α7 that differ from those in A-AChBP are colored in

orange for the (+) face and light blue for the (-) face and labeled with italics. Other color codes as in panel B.

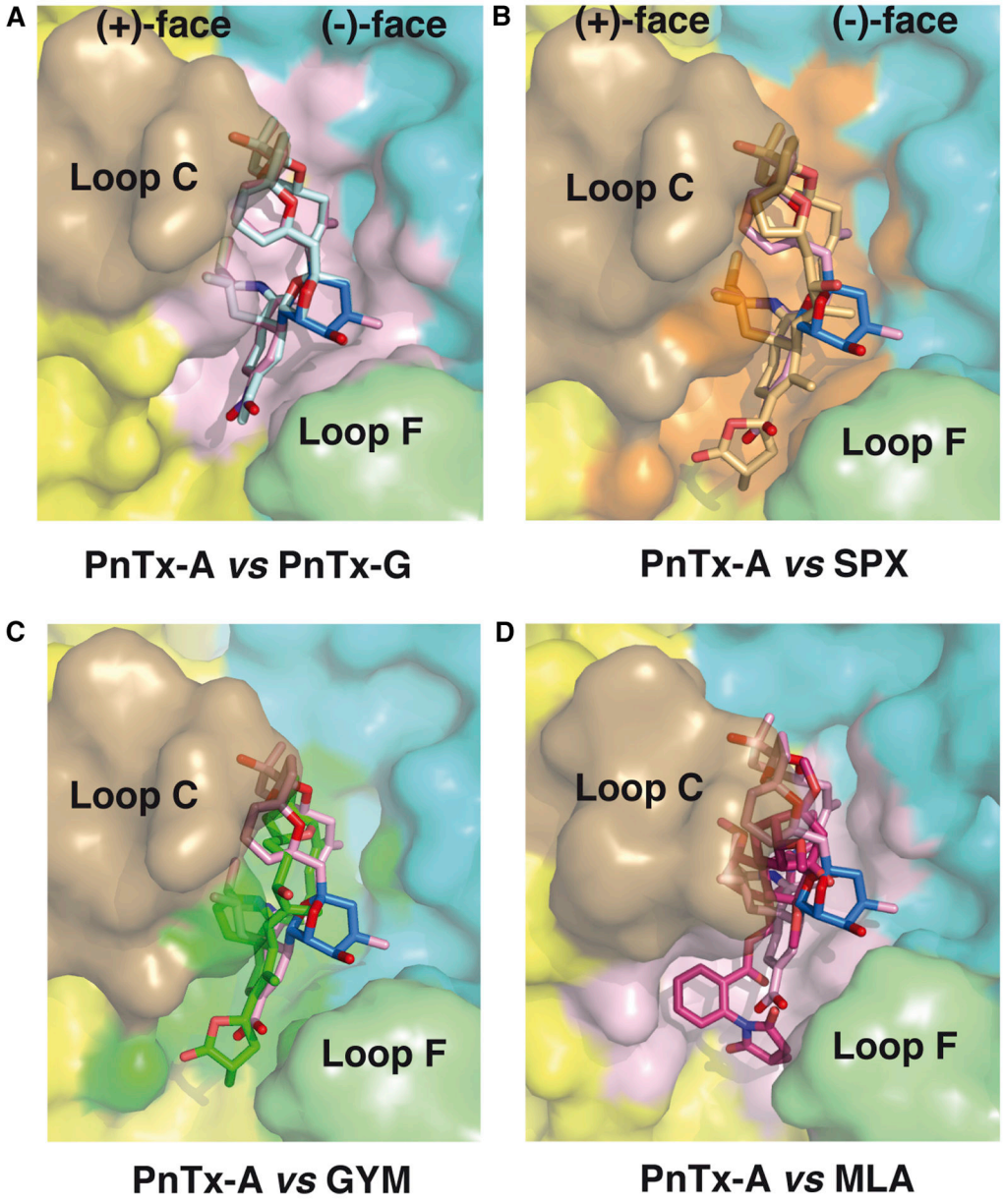

Fig. 4. Surface complementarity of bound PnTx-A and PnTx-G with the A-AChBP subunit interface and comparison with the SPX, GYM and MLA complexes

(A) The molecular surface buried by bound PnTx-A (pink toxin and surface) and PnTx-G (light blue toxin) at the (+) (yellow) and (−) (blue) faces of the A-AChBP subunit interface, is viewed radially from the pentamer outer periphery (transparent brown loop C, green loop F).

(B–D) Superimposition of PnTx-A (pink toxin) with SPX (orange toxin and surface), GYM (green toxin and surface) and MLA (magenta toxin and surface) as bound to A-AChBP. Compared with the accommodation modes of SPX and GYM within the ligand-binding pocket, the additional contact points with loop F residues mediated by the 5,6-bicycloketal

ring (blue) found in PnTx-A are evident. In contrast, the N-phenyl succinimide moiety of MLA extends to the bottom of the binding pocket.

Table 1

Inhibition constants (IC_{50}) for pinnatoxin effect on ACh-evoked nicotinic currents, recorded from oocytes either expressing the human neuronal α7 or α4β2 nAChR subtypes or transplanted with the muscle-type $\alpha 1_2\beta\gamma\delta$ nAChR.

nAChR subtype	IC_{50} (nM) [a]		
	PnTx-A [b]	PnTx-G	PnTx-A AK [c]
α7 (human)	0.107 (0.086 – 0.132)	5.06 [b] (3.84 – 6.67)	182 500 (2213 – 1 505 000)
α4β2 (human)	30.4 (19.4 – 47.5)	4.90 (3.97 – 6.06)	>1 000 000
$\alpha 1_2\beta\gamma\delta$ (*Torpedo*)	5.53 (4.5 – 6.8)	3.82 (2.99 – 4.88)	24 760 (9771 – 62 750)

[a] Values from individual experiments performed in triplicate or quadruplicate, with 95% confidence intervals provided in parentheses. The experimental curves associated with the data displayed on a grey background are reported as Suppl. Fig. S2A.

[b] From (Aráoz et al., 2011)

[c] See Fig. 3 in (Aráoz et al., 2011)

Table 2

Binding constants (K_i) for pinnatoxin binding on cells expressing the neuronal and muscle-type nAChRs, determined by competition against binding of ^{125}I-BgTx (α7/5-HT3, $\alpha1_2\beta\gamma\delta$) or [^{3}H]-EPI (α4β2, α3β2) at equilibrium.

nAChR subtype	K_i (nM) [a]		
	PnTx-A [b]	PnTx-G	PnTx-A AK [b]
α7/5-HT3 chimera (chick)	0.35 ± 0.04	0.72 ± 0.03	>10 000
α4β2 (human)	15.6 ± 5.2	101 ± 30	>2000
α3β2 (human)	9.4 ± 1.9	63.9 ± 1.2	>2000
$\alpha1_2\beta\gamma\delta$ (*Torpedo*)	2.8 ± 0.03	0.11 ± 0.04	>1000

[a] Average ± variation or means ± SEM from two to five distinct experiments performed in duplicate. Experimental curves associated with the data displayed on a grey background are reported as Suppl. Fig. S2B.

[b] From (Aráoz et al., 2011)

Table 3

Dissociation constants determined at equilibrium ($K_{d/equ}$) for pinnatoxin binding to Ca^{2+} sensing cells stably expressing the full-length α7 and α4β2 nAChRs, determined by competition against [^{3}H]-EPI binding.

nAChR subtype	PnTx-A $K_{d/equ}$ (nM)		PnTx-G $K_{d/equ}$ (nM)	
	Competitive component	Non-competitive component	Competitive component	Non-competitive component
α7 (human)	0.18 ± 0.10 [a]	2.6 ± 1.3 [a]	34 ± 4 [a]	270 ± 50 [a]
α4β2 (human)	95 ± 11 [b]	199 ± 1 [b]	99 ± 50 [a]	87 ± 62 [a]

[a] Means ± SD from three to four distinct experiments performed in triplicate

[b] Average ± variation from two distinct experiments performed in triplicate

Table 4

Kinetic constants for association and dissociation (k_{on}, k_{off}), calculated dissociation constants ($K_{d/calc}$), and dissociation constants determined at equilibrium ($K_{d/equ}$) for pinnatoxin binding to purified soluble AChBPs and AChBP/α7 chimera, determined by competition against binding of [^{3}H]-EPI (L-AChBP, A-AChBP/α7 chimera) or ^{3}H-MLA (A-AChBP).

AChBP/nAChR subtype	Kinetic/equilibrium parameters	PnTx-A	PnTx-G	PnTx-A AK
L-AChBP	k_{on} (10^9 $M^{-1}min^{-1}$)	0.21 ± 0.09 [a]	0.17 ± 0.01 [b]	nd
	k_{off} (min^{-1})	31.6 ± 7.9 [a]	60 ± 30 [b]	nd
	$K_{d/calc}$ (nM)	170 ± 77	360 ± 210	nd
	$K_{d/equ}$ (nM)	nd	(SPA) 315 [b]	(SFC) 88 000 ± 14 000 [b]
A-AChBP	k_{on} (10^9 $M^{-1}min^{-1}$)	1.4 ± 0.7 [a]	0.91 ± 0.03 [b]	nd
	k_{off} (min^{-1})	< 0.06 [b]	0.78 ± 0.06 [b]	nd
	$K_{d/calc}$ (nM)	< 0.05	0.86 ± 0.09	nd
	$K_{d/equ}$ (nM)	nd	nd	(SFC) 46 000 ± 4000 [b]
A-AChBP/α7 chimera III	$K_{d/equ}$ (nM)	nd	174 ± 19 [a]	nd

[a] Means ± SD from more than two distinct experiments performed in triplicate

[b] Single value from a single experiment performed in triplicate

[c] Average ± variation from two distinct experiments performed in triplicate

nd: not determined

SPA: scintillation proximity assay

SFC: stopped-flow competition